2

Solar explosive activity throughout the evolution of the solar system

RACHEL OSTEN

The time scales on which the Sun varies range from seconds to billions of years. Explosive events on the Sun involve the changing of magnetic configurations and subsequent liberation of energy, and processes associated with this energy transformation occur on the shortest of these time scales. However, the nature of the explosive events can change over the course of the Sun's evolutionary lifetime. This chapter covers the history of explosive events throughout the evolution of the solar system, with a focus on the observed manifestations of explosive events and what we can learn by studying them. Chapters in other volumes of this series (see Table 1.2) address parts of this topic. Chapter 2 of Vol. III describes the long-term evolution of magnetic activity of Sun-like stars, and Ch. 5 of Vol. II discusses observations of solar and stellar eruptions, flares, and jets. A description of radiative signatures of accelerated particles (primarily with application to solar flares) can be found in Ch. 4 of Vol. II, while Ch. 6 of that volume tackles models of coronal mass ejections and flares.

While the main theme of this chapter is the changing nature of these explosive events over evolutionary time scales, the influence of other important stellar parameters – such as rotation rate, convection zone depth, and the influence of binarity on rotation – are also discussed where appropriate. The focus of the chapter is to use an event-driven discussion of explosive events, keeping in mind how the parameters change with some key stellar parameters. This treatment is meant to illustrate key properties of explosive events that are known in stars of these age ranges.

An explosive event is made up of several distinct components, from energetic particles to coronal mass ejections to flares. While on the Sun these three components can be studied separately, on stars other than the Sun the identification and study of explosive events is limited to the radiative manifestation of the event, namely stellar flares. As diagnosed from the Sun, flares involve particle acceleration and plasma heating. They occur as a consequence of magnetic

reconnection somewhere in the outer atmosphere, yet involve all stellar atmospheric layers. Owing to a diversity of physical processes involved, they produce emissions across the electromagnetic spectrum, that for the Sun have been recorded from km-wavelength radio waves to the highest-energy gamma-rays.

A fundamental part of the solar–stellar connection (and the rationale for this chapter) is the assumption that processes studied in detail on the Sun are also operating on other stars, and that the differences can be related to fundamental physical differences between the stars.

The major sections in this chapter discuss events according to the ages of the stars. We begin with a review of processes likely to have consequences for planetary climates and space weather, referencing chapters in Vols. I–III as appropriate, and supplementing those chapters with information specific to diagnosing time-variable emissions. We begin with a brief mention of processes on evolutionary time scales, hearkening to what has been discussed in other chapters. Flares have been discussed in other reviews: see Benz and Güdel (2010) for an in-depth characterization of flares on the Sun and stars; Güdel (2007) provides a review of especially magnetic activity characteristics of the Sun in time; Shibata and Magara (2011) reviewed magnetohydrodynamic processes occurring during solar (and by extension, stellar) flares. This chapter's focus is unique, being driven by a discussion of the events themselves and how key stellar parameters, notably stellar age, control their characteristics.

2.1 Key parameters important to a discussion of explosive events

There are stellar parameters whose influence is important to understand. In addition, understanding the information that can be extracted from studies of flares at multiple wavelengths is necessary to studying these events. Table 2.1 gives an idea of how flares in some of these kinds of stars differ from those on the Sun and from each other, in terms of energetics, duration, and increases in intensity at visible wavelengths and X-ray wavelengths.

Table 2.1 *Comparing large solar and stellar flares*

	Energy (erg)	Max. duration	Intensity increase (visible)	Relative intensity increase in X-rays
Sun	10^{32}	~5 h	1.000 270	6000×
M dwarfs	10^{35}	several days	1000×	1000×
Young stars	10^{36}	~1 day	small	50×
Close binaries	10^{38}	~week	1.2	120×

2.1.1 Stellar parameters

What are the key stellar parameters to consider in this discussion of explosive events on solar-type stars? First, let us define what we mean by "solar-type stars" (see also Ch. 2 in Vol. III). Stars are characterized by their spectral type, which essentially is a measure of their surface temperature or their color, going from hot to cool: for a long time, the spectral types were O, B, A, F, G, K, and M, but recently types L, T, and Y were added to describe even cooler stellar objects. Another characterization differentiates by surface gravity; those we refer to here are main-sequence stars (or dwarf stars) and evolved or giant stars, with a class of moderately evolved subgiants in between. What makes stars of solar type is that they have an outer convective envelope that starts from early-F to mid-F (depending on gravity) and ranges ever deeper as we move towards cooler (or "later") spectral type, until the stars become fully convective by about mid-M-type dwarfs. Because all such stars lie on one side of a brightness–temperature (or magnitude–color) diagram (known as the Hertzsprung–Russell or HR diagram (such as Fig. 2.8 in Vol. III), they are generally referred to as "cool stars".

Explosive events on cool stars at their heart are powered by changing magnetic configurations in the stellar outer atmosphere and consequent liberation of energy. They are thus a manifestation of magnetic activity, and ultimately relate to dynamo processes in the stellar interior generating magnetic fields. Age and rotation are coupled because of the well-known stellar spin-down with time, often referred to as the "Skumanich $t^{-1/2}$ law" (see also Ch. 2 in Vol. III). In co-eval stellar clusters there is a spread of rotation at a fixed age, and the magnitude of this spread decreases with advancing stellar age (Ayres, 1997, and references therein). Stars are born rotating rapidly because of the conservation of angular momentum in the compression of the cloud out of which the star is formed (e.g., Chs. 2 and 3 in Vol. III). Rapid rotation engenders enhanced magnetic activity. Coronal structures produced as a result of this magnetic activity provide a torque that can spin the star down, as well as mass loss through a stellar wind in open magnetic field structures which can remove angular momentum from the star. Rotation and activity are fundamentally coupled, and an age–activity relation arises from the rotation and age relationship.

Rotation is not the only factor controlling magnetic activity. Convection zone depth, or its overturn time, also influences the ability of the star to generate vigorous and efficient magnetic fields (Noyes *et al.*, 1984). Because of the internal structure of stars in the cool half of the Hertzsprung–Russell (HR) diagram, outer convection zone depth traces mass, at least for stars less than about 1.2 solar masses, and down to the limit at which stars become fully convective, about 0.3 $M_\odot$ (e.g., Ch. 2 in Vol. III). The Rossby number, $R_0 = P_{rot}/\tau_{conv}$, which gives the

dimensionless ratio of stellar rotation period to convective turnover time, connects rotation, convection, and magnetic activity in cool stars on the main sequence. The dynamo generation of magnetic fields by dynamo action is driven by an interplay between rotation and convection (Charbonneau, 2010).

Explosive events occur as the result of liberation of energy from a changing magnetic field configuration, and characteristic magnetic flux densities in stars, where they can be measured independently, correlate with coronal emission. This is not really an independent variable, because age, rotation, and convection zone depth all drive the ability of the star to generate sufficiently strong magnetic field that covers a large fraction of the star.

Rotation rates may be affected by the presence of a stellar companion: for cool stellar binaries with separations less than about 10 stellar radii the time scales for synchronization and circularization are short enough that tidal locking effects dominate (Zahn, 1989), and a binary can maintain fast rotation for longer ages than a single star can.

We focus on stars on or near the main sequence in this discussion, but it is interesting to note that the radiative component of explosive events, with characteristics similar to those seen on the Sun, have been found on evolved stars. The usual explanations involved enhanced rotation due to the presence of a binary companion (the so-called RS CVn and Algol systems, with the latter having an additional complication of mass transfer taking place), or to engulfment of a companion (the single active evolved stars known as FK Com systems). Stars that start out life as intermediate-mass, non-convective stars can develop a thin outer convection zone as they evolve into the cool half of the HR diagram during their giant phase; they retain the fast rotation from their time on the main sequence and have exhibited flares (Ayres *et al.*, 1999). Flares have also been detected on intermediate mass stars after their ascent up and return down the giant branch (Ayres *et al.*, 2001), although the means by which the return of magnetic activity happens is less clear in this case.

2.1.2 Wavelength-dependent parameters

This chapter is event focused, so a discussion of the key parameters that can be extracted from observations of explosive events at a variety of wavelength regions where stellar explosive events are most studied is appropriate.

Table 2.2 summarizes the commonalities in manifestations of solar and stellar eruptive events. Stellar flares are not observed panchromatically (because there are no stellar spectral irradiance monitors), so these commonalities are built on a wavelength region by wavelength region basis, and on a star by star basis, with a sampling bias because some types of stars are more often observed for their

Table 2.2 *Solar/stellar explosive event commonalities*

Manifestation	Solar events	Stellar events[a]	Emission seen outside of flares?
	Impulsive phase		
Non-thermal hard X-ray emission	✔	?	no
Radio gyrosynchrotron/synchrotron	✔	✔	yes
Coherent radio emission	✔	✔	no
Transition region far-ultraviolet lines	✔	✔	yes
Hot black body optical/UV continuum	✔	✔	no
Coronal mass ejection	✔	?	no
Solar energetic particles	✔	?	no
	Gradual phase		
Coronal emission	✔	✔	yes
Optical chromospheric lines	✔	✔	yes

[a]Across different types of stars.

flares (e.g., M-type dwarfs). The picture that emerges, however, is generally one of agreement between the basic physical processes at work in solar and stellar explosive events.

Many flare tracers also exist outside times of flares, with a variation in degree. As an example, emission lines and continuum from the corona are seen in quiescence and in flares, with an increase in both line and continuum intensity during the flare (the amount of increase of lines and continuum depends on the flare temperature). Other flare tracers are unique to the flare event and point to a variation in kind. An example of this is the blue–optical continuum which forms during a white-light flare, and is not seen outside of any flare-like increase in visible light. The nature of these flare diagnostics, as to a change of degree or kind, are noted in Table 2.2.

An individual flare can be divided into two main phases: impulsive and gradual. This generally refers to the timing of emissions relative to the processes thought to be occurring in the flare. In the standard picture, the initial energy conversion caused by magnetic reconnection powers particle acceleration and possibly – depending on the energetics and on the magnetic configurations – a mass ejection. The downward-directed particles become trapped in loops and emit non-thermal incoherent radio emission (see Ch. 4 of Vol. III). Coherently emitting particles can be traveling either upwards out of the atmosphere or downwards into the atmosphere. Once the trapped particles precipitate from the magnetic trap, they deposit their energy in or just above the photosphere, producing thick-target non-thermal bremsstrahlung emission. This energy deposition results in the

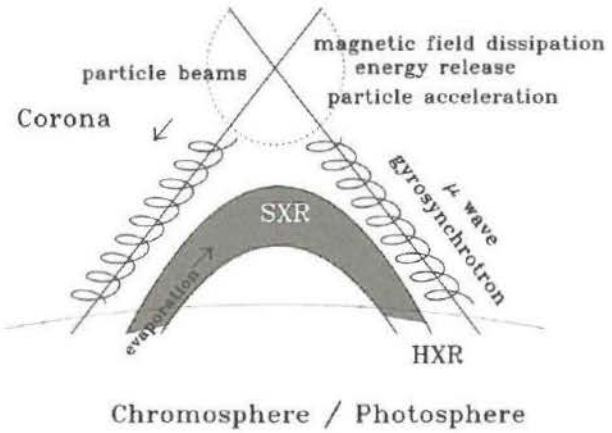

Fig. 2.1 Schematic arrangement in the outer atmosphere of the Sun or a comparable cool star indicating the flow of energy during a flare: a flare starts with magnetic reconnection high in the atmosphere that accelerates particles, leading to motion along field lines upward away from or downward towards the visible surface. Resulting emissions include hard X-rays (HXR), soft X-rays (SXR), and microwave emission. (Figure from Osten, 2002.)

heating of the photospheric material to temperatures near 10^4 K, and emissions from far-ultraviolet (FUV) lines. All of this is associated with the impulsive phase of the flare. The flow of energy at this point proceeds back into the upper atmosphere, with line emission from the lower chromosphere. Thermal X-ray emission occurs as well. As the energy input into the system decreases, emissions of all flare components return to the pre-flare level (see Fig. 2.1).

2.1.2.1 Correlations among multi-wavelength flare emissions

The processes involved in an explosive event occur across different layers of the stellar atmosphere, which respond with differing time scales to the time-dependent flow of energy in the explosive event. This leads to a number of expected correlations between facets of the event. Seeing these correlations in stellar flares gives support to the interpretation of the stellar flares using a solar flare scenario.

The Neupert Effect relationship is often used in stellar multi-wavelength flare studies to establish concordance with or likely disagreement with solar-flare models. It was formulated originally to describe the integral relationship between markers in a solar flare corresponding to the action of non-thermal particles, and the response from the atmosphere to the deposition of energy from these particles as it appears in coronal radiation. Written more generally,

$$L_{\text{gradual}}(t) \propto \int_{t_0}^{t} L_{\text{impulsive}}(t')\ dt', \tag{2.1}$$

where $L_{\text{impulsive}}(t')$ is the time variation of an impulsive phase process which diagnoses the presence and action of particles accelerated in the explosive event (for stellar studies usually radio gyrosynchrotron, transition region FUV emission lines, or photospheric UV–optical continuum emissions), and $L_{\text{gradual}}(t)$ is the intensity corresponding to the gradual phase (usually coronal emission, but some chromospheric emission lines display the Neupert Effect as well). The interpretation is that the gradual phase emission is responding to the buildup of energy that occurs as a result of the energy deposition being diagnosed by the impulsive phase emission. Correspondences in this "expected" manner are often used to bolster support for an interpretation of a stellar explosive event following the solar model. It is important to note, though, that there are also instances where the *opposite* behavior is observed in stellar flares (gradual phase emission leading the impulsive phase; see, for example, Bower *et al.*, 2003; Osten *et al.*, 2000). And not all solar flares follow the standard flare scenario.

Scalings between flare emissions occurring in different parts of the stellar atmosphere are also used to establish the validity of the solar flare interpretation. Butler *et al.* (1988) showed a linear relationship between the integrated energy emitted from the corona and from the chromosphere, both delineating the gradual phase of a flare. The interpretation into the tight correlation between two emission diagnostics with a large difference in formation temperature ($\sim 10^4$ K for chromospheric Hγ to 10^7 K for coronal X-ray emission) may originate from heating by X-ray back warming (see discussion in Hawley *et al.*, 2003). Kowalski *et al.* (2013) showed that the chromospheric Ca II K line showed a delayed response compared to the Balmer lines, and exhibited a Neupert-like effect with the impulsive flare markers.

There is often a close association between individual impulsive phase markers. FUV emission lines and optical continuum emissions have a similar temporal relationship (Hawley *et al.*, 2003). In principle the radio and optical components of a flare should behave similarly, as it is thought that they have a common origin in the action of accelerated particles. The radio emission is formed directly as the result of trapped electrons accelerated in the presence of a magnetic field, whereas the optical emission and other impulsive tracers are formed after energetic electrons precipitate from the magnetic trap and interact with material lower in the atmosphere. Figure 2.2 shows an example of a large radio flare occurring at the same time as a moderately large optical flare. In practice, because there are two emission mechanisms which can produce radiation in the cm-wavelength range, the interpretation of the radio light curve is not straightforward. As described in Sect. 2.1.2.3, circular polarization can be used as a discriminant between incoherent flare gyrosynchrotron emission (which should have little circular polarization) and coherent emission (which is often 100% circularly polarized). Gagne *et al.* (1998) and Osten *et al.* (2004) found that unpolarized radio flares had a higher rate

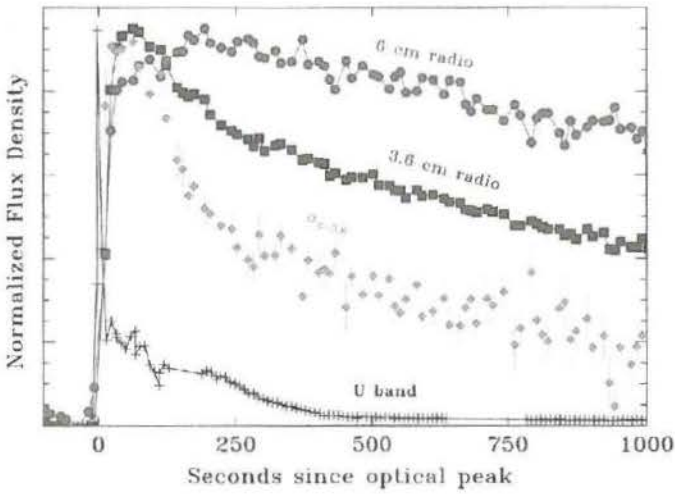

Fig. 2.2 Example radio-optical flare seen on the nearby M dwarf flare star EV Lac (from Osten *et al.*, 2005). Circles and squares show time evolution of radio flux density at wavelengths of 6 and 3.6 cm, respectively. Diamonds show the time variation of the radio spectral index, a measure of the relative strength of emission at the two wavelengths. The plus symbols show the temporal variability of optical emission in the U filter (cf. Fig. 2.5). Because the radio flux arises due to gyrosynchrotron emission from a population of accelerated particles, and the optical emission originates from a black body formed as the result of deposition of accelerated particles in the lower stellar atmosphere, one expects to see a temporal correlation between the two, which is observed for this flare.

of association with optical flares or other impulsive phase flare markers than the polarized radio flares.

2.1.2.2 Non-thermal hard X-ray emission

Chapter 4 of Vol. II discusses non-thermal bremsstrahlung hard X-ray emission from solar flares, and that same mechanism is believed to operate in stellar flares as well. This emission component originates due to the acceleration of electrons in the flare, and is not detectable outside of flares (on the Sun).

Optically thin non-thermal hard X-ray emission is important because it allows for the determination of the properties of the accelerated electrons (their energy distribution, and thus the total kinetic energy of accelerated electrons) in the flare. Yet, with the exception of one exceptionally bright stellar flare detected out to photon energies of $\approx$200 keV (see Fig. 5.11 of Vol. II), this flare signature remains elusive in stellar flares. Part of this stems from the inefficiency of non-thermal bremsstrahlung emission compared with thermal emission, being a factor of $\sim 10^5$ weaker. Another factor that has affected detections of non-thermal hard X-ray

emission from stellar flares is the tendency for these flares to show evidence of very hot, *thermal* plasma at temperatures up to and exceeding 100 MK (compared with peak temperatures of ~20 MK for solar flares). The sensitivity of astronomical hard X-ray detectors typically falls off above a few tens of keV, meaning that the tail of thermal emission from the hot plasma can easily overwhelm any small non-thermal continuum signature which might be present.

2.1.2.3 Radio bursts

In general the description of radiation from energetic particles reviewed in Ch. 4 of Vol. II suffices for the case of stellar flares as well as solar flares. Both incoherent (mostly gyrosynchrotron) as well as coherent processes are observed in stellar flares.

Gyrosynchrotron emission is seen both during stellar flares and outside of them, leading to the suggestion that the "quiescent" emission is composed of decaying flares (White and Franciosini, 1995). Multi-frequency observations of gyrosynchrotron emission can be used to infer the spectral distribution of the accelerated particles if the emission is optically thin: the observed spectral index α (determined assuming the radio flux S_ν varies with frequency ν as $S_\nu \propto \nu^\alpha$) relates to the power-law index of the distribution of energetic particles. If the emission is optically thick, the variation of flux density with frequency can be used to determine the effective temperature of the emitting electrons, the size of the radio-emitting source, the magnetic field strength in the radio-emitting source, and the total number of accelerated electrons contributing to the emission, as well as their changes with time. See Osten *et al.* (2005) for an example analysis in a large radio flare on a nearby M dwarf.

Some of the largest stellar radio flares even show a rising component at high frequencies (above a few tens of GHz), attributable to synchrotron emission from highly relativistic particles (Massi *et al.*, 2006). Similar types of "Terahertz" flares have been observed on the Sun, but current explanations require extreme parameters to explain them using known emission mechanisms (Krucker *et al.*, 2013). This population of accelerated electrons is trapped within the magnetic loop and may represent electrons with MeV energies, far in excess of the electron energies usually producing incoherent radio flares.

Coherent emissions are only inferred when bursty (extremely time-variable) emission is observed. There are two main coherent mechanisms seen in solar flares and inferred for stellar flares: either plasma radiation or emissions deriving from a cyclotron maser process. Section 4.3.1.2 in Vol. II covers plasma radiation. Unlike most solar coherent emissions, those on stars are typically observed to be almost 100% circularly polarized. This and their short time scales – as small as 1 ms, which implies a high brightness temperature – are what lead to the classification

as coherent emission. They can have brightness temperatures far in excess of the upper limit on brightness temperature of 10^{12} K for incoherent emission, set by the balance between inverse Compton scattering and synchrotron radiative losses (Kellermann and Pauliny-Toth, 1969).

Information can be extracted from coherent radio bursts constraining some fundamental quantities by associating the observed radio frequency with one of two frequencies associated with the plasma: the electron gyrofrequency $\nu_B = 2.8 \times 10^6 B$ MHz, or the plasma frequency $\nu_p \approx 9000\sqrt{n_e}$ MHz. The relative location of the emission in the stellar atmosphere can then be found by using a spatial relationship for this emission; e.g., assuming that the density obeys a barometric law, and the base density and scale height can also be calculated. Some coherent radio bursts exhibit a simple structure in a plot of intensity versus frequency and time, wherein the burst drifts with time and frequency. In these cases, the observed drift rate can be related to the speed with which the exciter is traveling through the stellar atmosphere by using the relation

$$\frac{d\nu}{dt} = \frac{\partial \nu}{\partial n_e}\frac{\partial n_e}{\partial h}\frac{\partial h}{\partial s}\frac{\partial s}{\partial t}, \tag{2.2}$$

or

$$\frac{d\nu}{dt} = \frac{\partial \nu}{\partial B}\frac{\partial B}{\partial s}\frac{\partial s}{\partial t}, \tag{2.3}$$

where h is a radial distance from the stellar surface, and s is the path length traveled through the atmosphere. For a barometric atmosphere the first equation above reduces to $\dot{\nu} = \nu \cos\theta v_B/(2H_n)$, where v_B is the exciter speed whose motions cause the plasma radiation, H_n is the density scale height, and θ the angle between the propagation direction and the radial direction from the surface. If the coherent radio burst is due to cyclotron maser instability, then the drift rate of the radio bursts can be analyzed using the second equation above, which reduces to $\dot{\nu} \approx v_B \nu^{4/3}/(47 B_0^{1/3} \lambda_B)$, where the magnetic field geometry is assumed to be dipolar, λ_B is the length scale of the dipole field, and B_0 is the magnetic field strength in the radio-emitting source. The duration of individual bursts, if small enough, can be related to the collisional damping time scale and the thermal temperature of the plasma constrained. See discussion in Osten and Bastian (2008) for an example.

2.1.2.4 Transition-region far-ultraviolet lines

The magnetic transition region of a cool stellar atmosphere is the location where the plasma β, defined as

$$\beta = \frac{P_g}{P_{\text{mag}}}, \tag{2.4}$$

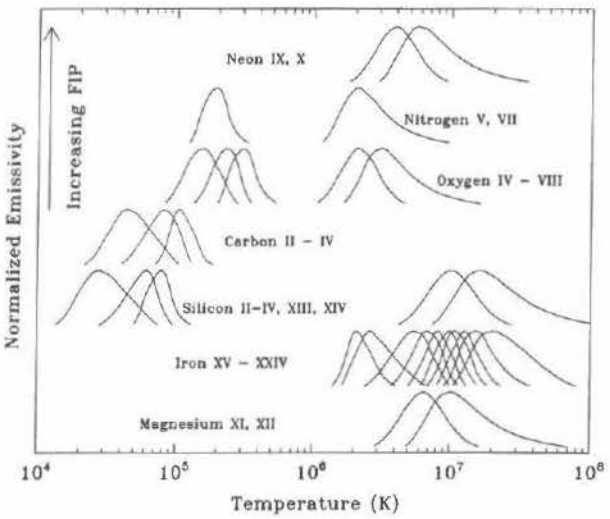

Fig. 2.3 Temperature coverage of chromospheric, transition region, and coronal lines from different elements and ionic stages obtained by combining spectra from ultraviolet through X-ray wavelengths; for the stellar case these instruments are the Space Telescope Imaging Spectrograph on the Hubble Space Telescope (HST/STIS), the Far-Ultraviolet Spectroscopic Explorer (FUSE), and the Chandra X-ray Observatory High Energy Transmission Grating Spectrometer (HETGS). The elements are ordered in terms of increasing first ionization potential (FIP), a quantity that gives the amount of energy required to remove the outermost electron from an atom of this element. These lines are formed under the conditions of collisional ionization equilibrium, and are generally optically thin, two conditions that permit inversion of their intensities to determine the temperature structure from the upper chromosphere to corona. (Figure from Osten, 2002.)

where P_g is the gas pressure and P_{mag} is the magnetic pressure, transitions from a value of $\gg 1$ in the lower atmosphere to $\ll 1$ in the upper stellar atmosphere. It separates the region in the lower atmosphere where gas pressures dominate dynamics from the upper atmosphere where magnetic pressure dominates. Transition region emission largely shows up in the far-ultraviolet (FUV) spectrum, and is dominated by emission lines from ionized species. The formation temperatures span a range, from about $10^{4.4}$ K to $10^{5.2}$ K, and represent stages from lithium-like ions to doubly ionized species. Figure 2.3 shows the temperature dependence of some transition region lines from ions of silicon, carbon, oxygen, and nitrogen. The plasma producing these transitions is considered to be in collisional ionization equilibrium, with the atomic process of collisional excitations being balanced by radiative de-excitations.

Transition region emission is seen during and outside of flares. During stellar flares these lines show an increase in the total intensity, as well as an increase in line

broadening. The transitions are for the most part optically thin, which together with being in collisional ionization equilibrium, means that the observed line intensity can be used to determine the volume emission measure of the emitting plasma. The volume emission measure, or VEM, is

$$\mathrm{VEM} = \int n_e n_H dV, \tag{2.5}$$

where n_e is the electron density, n_H the hydrogen density, and the integral is over the emitting volume V; the units of VEM are cm^{-3}. Examining the behavior of emission lines tracing different temperatures determines the multithermal nature of the flare. While often multiple temperatures are present, and responding to the flare energy input in this part of the atmosphere (see Fig. 2.4 for a flare in multiple chromospheric and transition region lines), there are examples of energy releases apparently confined to a small part of the atmosphere, as in the flare observed on the young solar analog star EK Dra (Ayres and France, 2010).

Time-resolved spectra with high enough spectral resolution reveal the presence of line broadening and line shifts during stellar flares. These measurements can be used to quantify the magnitude of turbulent motions in the atmosphere, and bulk flows, respectively. The increase in line broadening is parametrized as

$$\left(\frac{\Delta\lambda}{\lambda}\right)^2 = 3.07 \times 10^{-11} \left(\frac{2k_B T_{\max}}{m_i} + \xi^2 + v_{\mathrm{inst}}^2\right) \tag{2.6}$$

(after Wood *et al.*, 1997; Osten *et al.*, 2006), where $\Delta\lambda$ is the line profile width, λ is the wavelength of line center, k_B is Boltzmann's constant, $T_{\max}$ is the formation temperature of the line under conditions of ionization equilibrium, m_i is the ion mass, ξ is the most probable non-thermal velocity, and v_{inst} is the instrumental broadening of the line profile. Doppler velocity shifts to the line profile, if any, return information on the bulk flows using the standard Doppler shift formula. Blue shifts would be associated with material leaving the stellar surface (evaporation), and red shifts associated with material traveling from above the stellar surface back towards it (condensation).

2.1.2.5 Hot black-body UV/optical continuum

The impulsive (seconds–minutes) and often dramatic (factors up to 1000) increase in the white-light emission from M-type dwarf stars during flares was historically the first indication that stars were capable of producing short-time-scale flares as observed on the Sun. Because the spectral energy distribution of cool M-type dwarf stars (typically $T_{\mathrm{eff}} \sim 3000$ K) peaks towards longer visual wavelengths, the sudden increase in the blue–optical wavelengths seen during flares is easy to recognize. Figure 2.5 displays a representative optical spectrum of an M dwarf during and

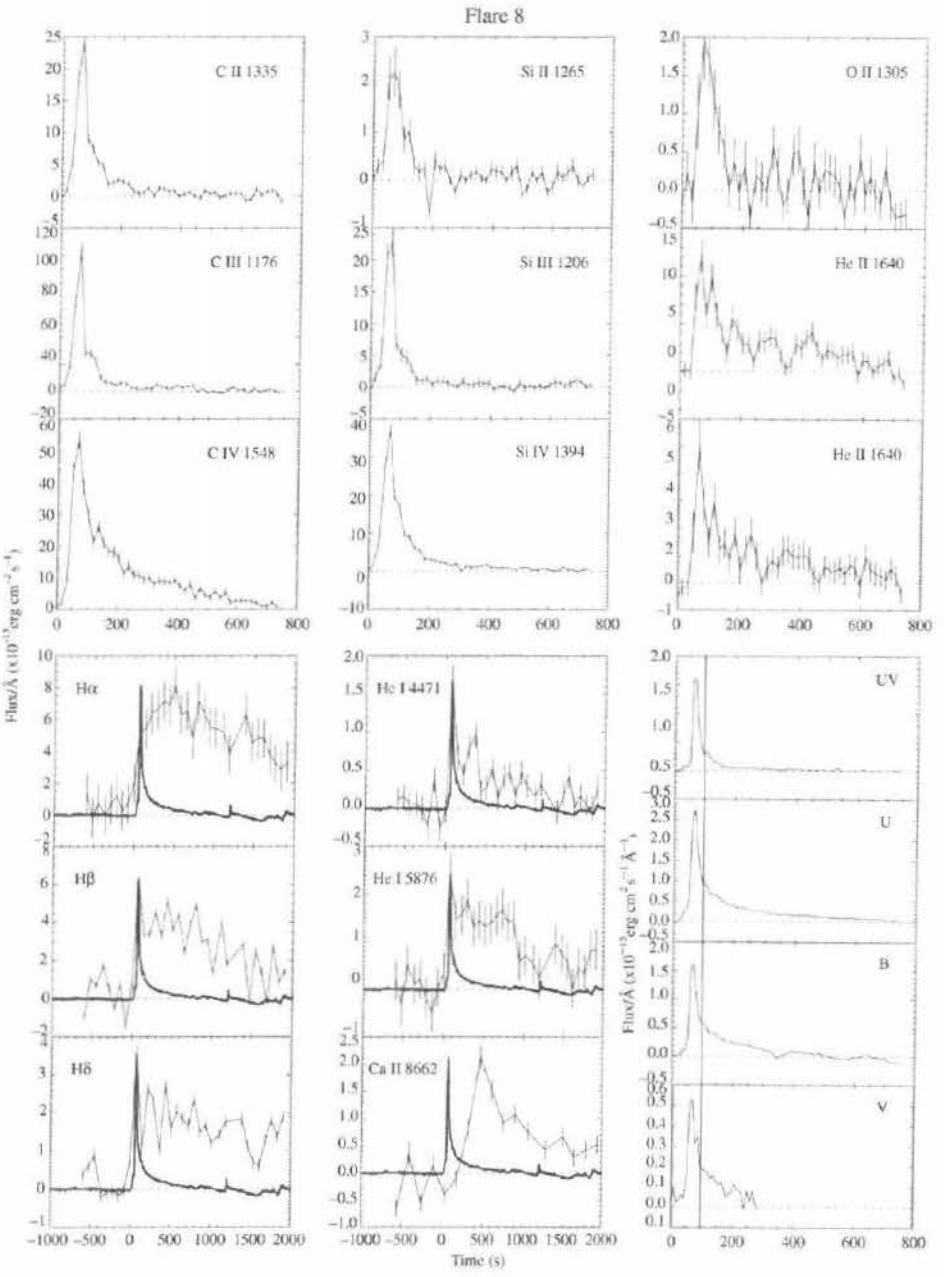

Fig. 2.4 Behavior of emission lines in the optical and ultraviolet during a well-studied flare on the nearby flare star AD Leo (from Hawley *et al.*, 2003). Ultraviolet emission lines (C II, Si II, O I, C III, Si III, He II, C IV, Si IV, N V) have time scales comparable to that seen in the broadband filters (UV, U, B, V) that measure primarily impulsive flare continuum emission. In contrast, the variation of emission lines originating from lower in the stellar atmosphere (Hα, Hβ, Hδ, He I, and Ca II) have a delayed response to the flare energy input seen from the hot black body, as well as a longer decay time scale.

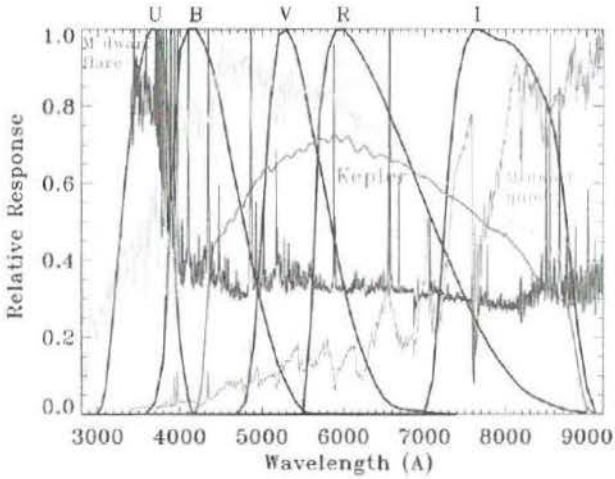

Fig. 2.5 Wavelength coverage of several standard filters used in optical astronomy, along with the wavelength coverage of the filter used in the Kepler mission. Overplotted are also spectral energy distributions of a quiescent and flaring M-dwarf atmosphere, taken from Kowalski *et al.* (2013). The solar spectrum is the 1985 Wehrli Standard Extraterrestrial Solar Irradiance Spectrum from http://rredc.nrel.gov/solar/spectra/am0/. A black and white version of this figure will appear in some formats. For the color version, please refer to the plate section.

outside of a flare; the rise in blue–optical continuum flux during the flare is evident. For reference, the wavelength coverage of some optical broadband filters are also shown: Johnson UVBRI filters, as well as the bandpass response used in the Kepler mission.

The spectral energy distribution of these white-light flares shows a dramatic change from that of the quiescent star. Broadband filters show a roughly black-body behavior, with the temperature of the black body near 10^4 K (Hawley *et al.*, 1995). The flare continuum can be diagnosed by relating the flare continuum flux to the black-body temperature and the area covered by the flare using the relation

$$F_\lambda = \frac{x R_\star^2}{d^2} \pi B_\lambda(T_{\rm BB}), \tag{2.7}$$

where F_λ, with units of erg cm^{-2} s^{-1} Å^{-1}, is the measured flare flux at effective wavelength λ, $R_\star$ is the stellar radius, d is the distance to the star, $T_{\rm BB}$ is the black-body temperature, and $B_\lambda(T_{\rm BB})$ is the Planck function evaluated at wavelength λ and temperature $T_{\rm BB}$. The factor x then gives the fractional area of the star covered by the flaring material, which for the most energetic flares approaches 10^{-3} of the total stellar surface (Hawley *et al.*, 2003).

Observationally, there is a close association between other impulsive phase flare signatures and optical/UV continuum increases. The black-body emission is thus thought to have its origins in the action of the accelerated electrons which dominate the impulsive phase. However, detailed modeling of the radiative hydrodynamic response of an M-dwarf atmosphere to the flare energy input specified by a solar-like prescription for electron-beam heating cannot reproduce the magnitude of observed flare enhancements in stellar flares because the electrons do not penetrate deeply enough into the stellar atmosphere (Allred *et al.*, 2006). The close observed correspondence between the white-light flare and signatures associated with accelerated particles (see discussion in Sect. 2.1.2.1) lends credence to the idea that accelerated particles are involved in the white-light flare. Then the key difference between solar and stellar white-light flares may be the applicability of a solar-type electron beam.

Although this flare signature has been studied most often from flares on M dwarfs, the black-body blue–optical continuum shape may be a common feature of white-light flares from more types of stars. Kretzschmar (2011) performed a superposed epoch analysis for solar white-light flares and detected signals corresponding to small enhancements at the times of even moderate (C-class) solar flares. The spectral signature, taken from a few broadband optical filters, appears to be consistent with continuum emission of black-body shape characterized by a temperature of about 9000 K.

Traditionally, the cool K and M dwarfs have been studied the most for their optical flare signatures, due to the enhanced contrast with the underlying stellar emission. Other studies have expanded the stellar types where impulsive optical flares have been observed, from solar-type stars (Maehara *et al.*, 2012; Osten *et al.*, 2012) to the coolest M dwarfs (Stelzer *et al.*, 2006). There have even been reports of white-light flares on more massive A-type stars (Balona, 2012). The ability to make sensitive relative photometric measurements with a long observing time has enabled these advances. Future astronomical telescopes will use the time domain to find transiting exoplanets, enabling an exploitation of these data for finding new classes of flaring stars.

2.1.2.6 *Stellar coronal mass ejections*

Coronal mass ejections (CMEs) are an important component of many solar explosive events. Chapters 6 and 12 in Vol. II discuss models of solar CMEs and their relation to flares and the entirety of the eruptive event. Additionally, they are an important component of space weather. Solar studies have demonstrated that the kinetic energy of CMEs is of the same order as the bolometric radiated flare energy from a sample of solar eruptive flares (Emslie *et al.*, 2012).

Based on the close association between flares and CMEs on the Sun, and the apparent similarity in behavior between solar and stellar flares (albeit scaled up by orders of magnitude), it is natural to extrapolate scalings between solar flares and CMEs to investigate the impact of stellar CMEs. This is a speculative affair due to the fact there are no confirmed detections of stellar CMEs (Leitzinger *et al.*, 2011). The workhorse of solar CME observations is the coronagraph, but the requirements on sensitivity, time, and inner working angle so far have been prohibitive for astronomical coronagraphs. Other methods have been proposed, such as interpretation of varying hydrogen column densities in X-ray spectra obtained during flares (Franciosini *et al.*, 2001) or evidence for weak high-velocity features in the wings of optical emission lines during flares (Houdebine, 1996). Osten *et al.* (2013) speculated that a large drop in mid-IR flux from a star with a debris disk could have been caused by a massive CME from the star.

Several studies have established scaling relations between solar flares and CMEs and extrapolated to the case of stellar flares (see Sect. 4.2.2 for such scalings; also Aarnio *et al.*, 2012; Drake *et al.*, 2013). The implied total CME-driven stellar-mass loss for young active stars is high, at levels from 10^{-12}–$10^{-9}\,M_{\odot}\ \mathrm{yr}^{-1}$ (compared to about $3 \times 10^{-14}\,M_{\odot}\ \mathrm{yr}^{-1}$ for the total mass loss of the present-day Sun; see Ch. 2 in Vol. III). These high levels are at odds with constraints on stellar mass loss established for young solar-like stars (Matt and Pudritz, 2007). An apparent resolution to this conflict lies in a breakdown in the solar–stellar connection as regards stellar eruptive events, but this has not been demonstrated conclusively. Other signatures of CMEs in the electromagnetic spectrum that can be exploited are low-frequency type-II radio bursts, which have a distinctive signature of a burst which drifts in frequency and time as the MHD shock produced by the CME travels through the tenuous outer stellar atmosphere. The discussions in Chs. 4 and 5 of Vol. II provide more description of solar CMEs.

2.1.2.7 Stellar energetic particles

Solar eruptive events involve the production of energetic particles, which are observed throughout the solar system. Chapter 9 of Vol. II discusses energetic particles produced by solar eruptive events, which generally have kinetic energies in excess of 0.1 MeV/nucleon. The acceleration mechanisms in the solar case have their origin in either the flare process or in a shock associated with the coronal mass ejection, and the energies can extend up to 7 GeV/nucleon. In contrast to the accelerated particles observed in the solar atmosphere during the flare, which are generally electrons trapped in magnetic loops or ions observed at low heights in the solar corona, these energetic particles are outwardly directed from the star, and detected 1 AU or more from the Sun. We have no constraint on the presence of stellar energetic particles in astrospheres associated with stellar explosive

events. Application of scaling laws between solar flare X-ray photons and proton fluences are often used to explore parameter space for the influence of stellar explosive events from young stars in affecting material in the early solar nebula (the meteoritic isotopic abundance anomalies; Feigelson *et al.*, 2002), as well as the influence of eruptive events on habitability of extrasolar planets (Segura *et al.*, 2010). It is not clear how applicable these scaling laws are, and they do not (as yet) provide testable constraints for stellar cases.

2.1.2.8 X-ray flares

Stars produce X-ray emission during and outside of flares. The emission is well-described by a plasma in collisional ionization equilibrium, where ionic transitions with collisional excitations balanced by radiative de-excitations give rise to numerous emission lines in the extreme ultraviolet to X-ray spectral bandpass. Continuum emission contributes as well, predominantly from free-free emission but including free-bound and 2-photon processes (Dere *et al.*, 1997). Figure 2.3 shows the temperature coverage probed by the highly ionized species in the X-ray regime, at temperatures above 10^6 K. More description of the atomic physics involved in the production of this emission can be found in Mewe (1999). Spectral analysis of X-ray flares returns key quantities describing the spectral energy distribution of the flaring plasma: the plasma temperature and volume emission measure, and the abundances of the elements contributing significantly to the emission (C, N, O, Ne, Mg, Fe, Si, S for the most part). In situations where the spectral resolution is high enough, changes in the electron density of coronal plasma can be discerned during flares. A much more exhaustive review of stellar X-ray emission and flares in particular can be found in Güdel and Nazé (2009).

The major change in the emission during flares is the sudden creation of denser, hotter plasma, produced as the result of chromospheric evaporation lower in the atmosphere. Temperature and volume emission measure increase, with a characteristic increase during the rise phase of the flare and a return to quiescent conditions in the decay phase. Figure 2.6 shows an example X-ray flare seen on the tidally locked active binary system named TZ CrB (composed of two nearly solar-type stars with 1.1 day orbital/rotational periods) in the energy range 0.8–10 keV (1.2–16 Å). Outside of the flares plasma temperatures are already elevated compared to the Sun – quiescent temperatures of 20 MK are par for the course, while these temperatures are usually only achieved on the Sun during solar flares – and during stellar flares the temperature increases beyond that value, with maximum values around 10^8 K.

The abundance of the flaring coronal material can exhibit a change when compared against the abundance of non-flaring coronal material. Outside of flares, the X-ray spectrum of magnetically active stars typically shows abundances less than

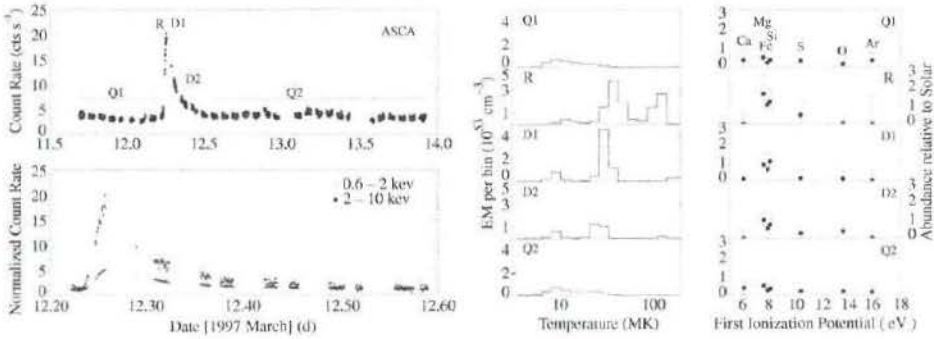

Fig. 2.6 Example stellar flare X-ray light curve (left panel), with the temporal segments analyzed spectroscopically identified. The panel below this total X-ray intensity light curve shows the time variation in two bandpasses: the harder energy bandpass is much more impulsive, reflecting the creation of very hot plasma during the flare rise phase. The right panel shows corresponding change of temperatures and abundances in the phases of the flare. This flare was observed on the active binary system TZ CrB, which is composed of two solar-like stars rotating at a period of 1.1 days (from Osten *et al.*, 2000).

the solar photospheric values (Brinkman *et al.*, 2001). During the rise phase of flares, the coronal abundances *increase*, signaling a temporary increase in material in the corona, presumably brought up from lower in the stellar atmosphere where the abundance is higher. This is in line with expectations from chromospheric evaporation and abundance patterns in coronal emission seen outside of flares, which in the most active stars show a lowered amount of low first ionization potential (FIP) elements compared to the solar photosphere. There are flares for which no change in abundance pattern occurs relative to the quiescent emission and the interpretation here is more complex (Osten *et al.*, 2010).

Indirect constraints on the length scales of stellar flaring coronal plasmas generally suggest length scales longer than those measured during solar coronal flares. The number of assumptions required to employ such techniques may affect the outcome. The VEM, a measurable parameter from spectral fitting, depends on electron density, ion density, and emitting volume, so with a constraint on VEM and an assumption about density and coronal geometry length scales can be estimated to first order. Other methods rely on applying a balance between radiative and conductive losses in the decay phase of the flare to derive a constraint on loop length (van den Oord *et al.*, 1988), or describe the change in stored magnetic energy with time using a simple prescription for the magnetic configuration (Kopp and Poletto, 1984). The most common application to describe length scales in stellar X-ray flares has been the work of Reale *et al.* (1997). The technique uses information on *e*-folding time scale in the decay phase of the flare light curve, as well as time-resolved spectral analysis of the change of temperature and volume emission measure with time. Assuming that the flare geometry and

hence volume do not change appreciably with time, the volume-emission measure changes can be related to changes of density. Hydrodynamic modeling of decaying flaring loops with a range of dimensions and time scales provides a quantification of the amount of heating occurring in the flare decay, which can be assessed observationally by the slope of the points in the temperature–density plane during the flare decay. As with most parametrized efforts, a single semi-circular loop with a constant cross-section is assumed for loop geometry. Hydrodynamic modeling of decaying flaring loops with a range of dimensions and time scales is folded into instrument response, allowing for a refinement of the estimates and application to specific instruments and bandpasses. The hydrodynamic method applied to solar flares returns values of flaring loop semi-lengths of $\sim 10^9$ cm, or $L/R_\odot \sim 0.01$, typical of solar active region flaring loops (Reale *et al.*, 1997). The method applied to stellar flares returns loop semi-lengths which are larger, in both an absolute sense and when compared against the radius of the star: Stelzer *et al.* (2006) analyzed a flare on a very low mass dwarf, finding a length scale of 1.4×10^{10} cm, or $L/R_\star \sim 2$, while Osten *et al.* (2010) dissected a flare on a higher-mass M dwarf, finding a slightly smaller length in absolute units, but a relative size scale of $L/R_\star \sim 0.4$ when considering the factor of $\approx$ three difference in radius of the two stars. The study of Favata *et al.* (2005) examined flares on young ($\sim$1 Myr-old) stars, and found loop semi-lengths as large as $\sim 10^{12}$ cm, exceeding the stellar radius by large values (factors of tens). Because of its simplicity and dependence on relatively easily derived observable parameters, this approach has been used most widely to diagnose length scales in stellar flaring coronal plasmas.

2.1.2.9 *Chromospheric lines*

Chromospheric emission lines originate in the gradual phase of the flare. As demonstrated in Fig. 2.4, these lines (like Hα) show a much longer decay time scale before returning to quiescent conditions than for markers of the impulsive phase. These lines also exhibit a delay in responding to the energy input: their intensity maxima occur significantly after that of the impulsive phase flare emission. These chromospheric lines are optically thick (in contrast to the transition region and coronal emission lines originating higher up in the stellar atmosphere) and so inferring physical conditions in the flaring atmosphere requires the use of radiative transfer models to describe how the radiation interacts with the material. Consideration of the changing conditions during a flare additionally needs a dynamical treatment, such as that in Allred *et al.* (2006).

2.1.2.10 *A note about energy partition within flares*

There are very few multi-wavelength observations of stellar flares where we can get an entire picture of an explosive event, including the energetics of the various

components described in the above sections. Even on the Sun this is only possible for the largest events, and even then some crucial pieces of information are missing and must be extrapolated (Emslie *et al.*, 2012). This requires stellar astronomers to rely on solar scalings that can be applied to stellar flares, or application of results from a detailed study of one stellar flare to flares on different types of stars. So when considering flare measurements made in one wavelength region, this energy release needs to be placed in context with what might be appearing in other regions of the electromagnetic spectrum. Nevertheless, a consistent picture does appear to emerge when considering the radiative output of solar and stellar flares. Kretzschmar (2011) showed that optical continuum flare radiation carries about 70% of the total radiative energy, as measured by total solar irradiance. Emslie *et al.* (2012) showed that X-ray radiated energy of solar flares accounts for about 20% of the total bolometric radiated energy. Multi-wavelength studies of M dwarf stellar flares (Hawley *et al.*, 1995) show similar ratios between the hot continuum radiation in the optical bandpass and soft X-ray radiated energy. The contribution to the flare energy from accelerated particles is less constrained in both solar and stellar flares due to lack of constraint of key parameters, but lower limits suggest that it may well exceed that in the radiated energy (Emslie *et al.*, 2012; Smith *et al.*, 2005).

2.1.3 Flares in aggregate

As examples of dissipative processes, stellar flares are expected to follow a power-law size distribution. Any wavelength region where flares exhibit emission can be used thus; however, in the coronal regime the size distribution of flares takes on added importance. The flare-size distribution is characterized by a power-law α such that

$$\frac{dN}{dE} = kE^{-\alpha}, \tag{2.8}$$

where dN/dE gives the number of flares occurring per unit time per unit energy, k is a constant, and E is the flare energy in the bandpass being considered. As noted by Parker (1988), for values of $\alpha > 2$ it is possible to integrate the contribution of smaller and smaller flares until the quiescent X-ray luminosity of the star is achieved. This is termed the "nanoflare heating hypothesis". This ensemble approach determines the relative importance of flares of different sizes. While many authors (notably X-ray astronomers) give a lot of importance to the value of α, the overall flare rate is also important. As Hilton (2011) demonstrated, M dwarfs with differing activity levels (from inactive to active to the most active M dwarfs) still produce flares, and with similar values of α, yet the overall flare rate can vary by orders of magnitude.

2.2 Time scales: explosive events on stars, young to old

Although age is one of a star's fundamental parameters it is also the most difficult to measure accurately. Soderblom (2010) provides a summary of the available techniques for age-dating stars and ensembles of stars. Each has its own advantages and drawbacks, and the uncertainty associated with a particular age measurement can vary widely. For the present purposes broad age categories are used to delineate some key times within the life of a star, and relate what is known about explosive events on stars within this range. It is important to remember that within each broad age category other parameters like stellar mass and rotation are important to consider, and for a variety of reasons the observational constraints that populate this parameter space suffer heavily from bias (in stellar type and wavelength regions) and observational limitations.

2.2.1 Stellar infancy: birth to the zero-age main sequence

Chapter 3 of Vol. III describes the formation and early evolution of stars and protoplanetary disks, and Fig. 1.1 of Ch. 1 in Vol. III gives key events in the history of the Sun. Although the age range in this first age category is only a percent or so of the total main-sequence lifetime of the star, there are several important steps to the life of the star that occur during this time. Before discussing what is known about explosive events on stars of this age range, it is necessary to set the stage of what is going on in stellar evolution, as the environment around the star influences how we observe and interpret explosive events. For this section we concentrate on ages ranging from stellar birth to the time it takes the star to reach the zero-age main sequence (ZAMS), at which point the star is in stable hydrostatic equilibrium, and there is negligible contribution to the stellar luminosity from any accretion-related processes. This time scale is a function of stellar mass, being approximately 50 Myr for a solar-mass star, and longer than 160 Myr for a star of 0.5 $M_\odot$ or less. For the purposes of discussion, and because stellar ages can be uncertain by factors of two or more, we include stars of ages up to ~100 Myr. The main point is to differentiate factors of stellar youth affecting explosive events from those associated with accretion and the remnants of the planet-forming disk.

A star is considered born when the fragmented molecular cloud has contracted to the point where it forms a hydrostatic core. Phases of star and planet formation are still continuing, and the star can be referred to generally as a pre-main-sequence star, because its location in the Hertzsprung–Russell diagram is above that of the ZAMS. A solar-mass pre-main-sequence star, for instance, has a larger stellar radius and lower gravity than an equal-mass star on the main sequence. At these early times the star is still enshrouded by a massive disk out of which it formed. Once the star+disk system has proceeded to the point that both components

contribute to the integrated light, the object can be referred to as a classical T Tauri star, or class-II object (see Evans *et al.*, 2009, for a "Diskionary" explaining different terms relevant to young stars). Accretion processes are still occurring, and the star is rotating rapidly due to its youth. As the disk disperses, the total light becomes dominated by the star itself, and these objects are referred to as weak-lined T Tauri stars or class-III objects. These stars might not show any evidence for a massive, gas-rich disk but it is still possible for them to host a weaker disk that is gas poor. The lifetime of the gas-rich disk has a systematic dependence on the mass of the star, with solar-mass stars losing their disk in ~5 Myr. However, there is a range of disk lifetimes within a given mass range: other factors such as multiplicity, proximity to the intense radiation field of O stars, and residing in a dense stellar cluster can each shorten the disk lifetime. The gas-poor or debris disks, are composed of rock, dust, and ice, which represent the end phase of the process of star formation. This phase can last for a long period of time, however; while the small particles (typically 1–100 μm in size) are subject to removal by radiation pressure from the star, or spiral in towards the star through Poynting–Robertson drag, these time scales are relatively short (of order 10 Myr), and other processes such as a collisional cascade of larger particles can replenish the disk. Increasingly sensitive astronomical detectors can also see evidence for faint increases in mid-infrared light above that expected from the stellar photosphere, signaling the presence of a debris disk at much older ages. Our solar system's asteroid and Kuiper belts would be considered late-time examples of debris disks.

Magnetic activity in general is at a high level in these young stars because of their rapid rotation, but the interpretation can be confused by other processes occurring in the system that have similar observational characteristics to magnetic reconnection processes. While explosive events produce temporal changes in luminosity, so too can accretion produce variable signatures of similar diagnostics. Feigelson and Montmerle (1999) discuss high-energy processes in these young stars. Observations of flares at X-ray and radio wavelengths are dominated by reconnection processes. The thermal coronal radiation showing up in X-rays does appear to follow patterns seen in older more active stars (temporal trends of intensity, temperature, VEM), and non-thermal radio gyrosynchrotron emission has a different spectral and temporal signature from radio thermal bremsstrahlung emission from an ionized wind of outflowing material from the star + disk. In contrast, observations of optical variability are more problematic to interpret, because accretion-related variability can also produce changes in continuum and Balmer-line emission similar to what is seen during flares on older more active stars. Because young stars are born in clusters, they tend to be spatially concentrated, which can make crowding in the field of view an issue, but the advantage of

multiplexing hundreds of stars in the field of view of an astronomical telescope to study stochastically occurring and relatively infrequent explosive events outweighs this concern for the most part.

Flares some 100–1000 times more energetic than the biggest solar flares occur roughly once a week on these young, rapidly spinning stars. Most studies have concentrated on singling out particular stars for further study, but there have been a few systematic studies of flaring in clusters. Wolk *et al.* (2005) studied X-ray flares on young suns in the Orion Nebula Cluster, with masses $0.9 \leq M \leq 1.2\ M_{\odot}$; these are pre-main-sequence stars with an age near 2 Myr, so for the most part they still have their accretion disk. The radiated energies span 10^{34}–10^{36} erg (to be contrasted with the largest solar flares approaching 10^{33}; Schrijver *et al.*, 2012), with a power-law distribution characterized by an index α of $\sim$1.7. The flare frequency in this sample is 1 flare per star every 650 ks after correcting for data gaps. The flare durations span 1 h to 3 days, with amplitudes generally less than about 10 times the underlying level. Stelzer *et al.* (2007) looked at X-ray flaring in young stars in the Taurus Molecular Cloud (with ages spanning 1–3 Myr). They also found energetic flares, with flares spanning the range of a few times 10^{33}–5×10^{35} erg. Flares with energies in excess of 10^{35} erg happen once per 800 ks per star, with a duration of 10 ks. They also found a power-law distribution of flare energies, with an index $\alpha = 2.4 \pm 0.5$. The level of flares to which such studies are sensitive is limited to those events which are far more energetic than the largest event observed on the Sun, due to the intrinsic limitation of astronomical detector sensitivity.

For these very energetic flares from stars in the range of a few Myr, stars with and without a gas-rich disk show no strong difference in flare rate, and there also does not appear to be a change in flare rate from solar mass to low mass stars. Stelzer *et al.* (2000) found no difference between X-ray flares on stars with and without an accretion disk in clusters with ages 1–3 Myr. Caramazza *et al.* (2007) compared the coronal flare frequency distributions of flares on solar-mass stars in Orion (0.9–1.2 $M_{\odot}$) with those of low mass stars (in the mass range 0.1–0.3 $M_{\odot}$) and found no difference in flaring behavior for stars as a function of mass. From a compilation of flares seen in Balmer emission lines and optical continuum, with flare energies in excess of 10^{33} erg, Guenther and Ball (1999) found a factor of two difference in the flare rate of stars with and without an accretion disk, with the flare rate for classical T Tauri stars (i.e., those with disks) about a factor of two lower than weak-lined T Tauri stars.

Over slightly longer evolutionary time scales there is a decrease in flare rate. The optical flare study of Guenther and Ball (1999) also included one pre-main-sequence star, and the flare rate of the ZAMS star was significantly reduced, by about a factor of 10 compared to the weak-lined T Tauri stars. Stelzer *et al.* (2000)

did a systematic study of the X-ray flare rates of T Tauri stars at ages 1–10 Myr, and studies of stars in the Pleiades (age ~100 Myr) and the Hyades (age ~600 Myr). They noted that the G stars in their group had the lowest flare rates by spectral type. Corrected for sensitivity biases, their flare rate for the Pleiades was 0.67±0.13%, for the Hyades 0.32±0.17%, expressed as a fraction of time in the flaring state compared to total observation time.

For the youngest stars, the loop lengths inferred from X-ray flare analysis may be much larger than seen on the Sun, and can provide a connection from the star to the disk. This is potentially important, as the flares can provide a source of turbulence to the disk and may affect planet formation. However, the measurement of flare loop lengths on stars, lacking spatial resolution, is model-dependent and relies of the applicability of the model. Favata *et al.* (2005) analyzed some of the largest flares from young stars in the Orion Nebula Cluster, without selecting mass ranges. From an analysis of the flare decays, and using a one-dimensional hydrodynamic loop model, which returns constraints on loop length, they found that a substantial number of large flares appeared to originate from flaring loops with lengths sufficient to connect the star to the planet-forming disk (and thus potentially increase the turbulence in the disk and affect planet formation). The loop lengths implied are several tens of stellar radii, compared with a fraction of solar radius for the largest flaring loops observed on the Sun. This idea has been investigated further with different samples of flares from pre-main-sequence stars. Just as other flare parameters show a distribution, there is a distribution of flare loop lengths. McCleary and Wolk (2011) found that the longest loop lengths were of order several stellar radii and tended to occur on stars with an infrared excess, indicating that they still possessed their planet-forming disk. Whether this is a cause and effect, or a result affected by over-extrapolation of a model beyond its bounds of applicability, is still being debated.

Studies of radio flaring on young stars occur more sporadically, but indicate a population of much more energetic electrons than usually seen in solar flares. One particular well-studied pre-main-sequence star, V773 Tau, shows energetic *synchrotron* flares, and this has also been seen on a few other young stars (Kóspál *et al.*, 2011; Getman *et al.*, 2011). In contrast, solar flares show less energetic gyrosynchrotron emission from lower harmonics of the gyrofrequency, indicating less energetic electrons. The periodic nature of the flares studied in detail has been explained as arising in an eccentric binary system where periastron passage of the secondary, and two extended magnetospheres, causes reconnection to high energies with a recurrence of approximately the orbital period. Whether this behavior is commonplace among young stellar objects or limited to binary systems satisfying these conditions is a current topic of investigation. It does indicate a role for

MeV-level electrons in the explosive event, which may be important in explaining meteoritic abundance anomalies.

Observations of isolated young stars confirm the general pattern of elevated activity in young stars seen in clusters, but show some marked differences from solar behaviors: steeper flare frequency distributions, flares limited in temperature/wavelength region, and multi-wavelength flare signatures exhibiting the opposite trend to the standard solar flare scenario. The nearby G star EK Dra is a solar analog with an estimated age of 50–70 Myr, placing it in the age range under consideration. The distribution of its high-energy flares have been characterized as a power-law with α of 2.08±0.34 above an energy of $10^{30.2}$ erg (Audard *et al.*, 2000). Guedel *et al.* (1995) found radio variability in this object that was interpreted as flares, but the observations were not sensitive enough to perform a detailed study of their characteristics. Ayres and France (2010) found a transient UV event on this star seen only in Si IV but not in a coronal line found in the far-ultraviolet bandpass. Whether this last example can even be counted as a component of an explosive event is not clear, because its formation in a narrow temperature range in the upper atmosphere (and without any apparent contribution from high-energy emission) suggests a limited physical range for energy deposition. Feigelson *et al.* (1994) studied V773 Tau, a classical T Tauri star, in which a radio flare was observed without any apparent X-ray variations. Similar behavior was noted in a cool star serendipitously observed in outburst at mm wavelengths in the Orion Nebula Cluster, in which the X-ray flare preceded an accompanying radio outburst from the star (see Fig. 2.7).

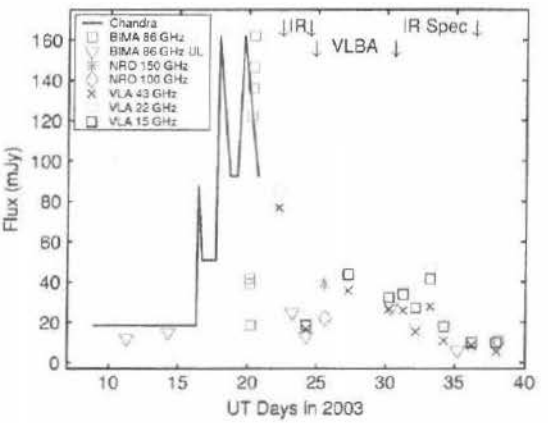

Fig. 2.7 Unusual radio/X-ray flare observed on a pre-main-sequence K-type star in the Orion Nebula. The strong outburst was observed first at X-ray wavelengths, then at radio wavelengths, in contradiction to the pattern usually seen for solar explosive events. Figure from Bower *et al.* (2003).

2.2.2 Stellar teenage years: ZAMS–1 Gyr

At this phase in a star's evolution, rapid rotation is still an important factor, although it has declined since the star's youth. According to the Skumanich $t^{-1/2}$ relation between age and rotation, a solar-mass star would have a rotation rate that is only a factor of 2–7 above the Sun's present-day rotation; activity that accompanies the faster rotation should be enhanced, but below the extremes represented by the youngest stars. Earlier-type cool stars spin-down faster than lower-mass stars (Stauffer, 1991), so by these ages M dwarfs dominate the samples of active stars. The general decrease in activity levels compared to the extremes seen at young ages means that capturing flaring activity on stars of this age range (with the exception of M dwarfs) is more difficult to do systematically, and consequently there is a heavy bias towards the lower-mass end in observations of flares on stars of this age range. The fact that M dwarfs are the most common type of star based on mass functions also contributes to this bias. There are open clusters (notably the Hyades at an age of ~800 Myr) which are nearby enough for sensitive studies of explosive events, although they are spatially dispersed compared to star-forming regions and this makes it difficult to capture more than one or two objects in the field of view of typical astronomical telescopes.

The possible dependence of stellar flare rate on evolutionary age can be explored by combining scaling relations between flare frequency and underlying coronal emission with those relating coronal and chromospheric emission, and others describing the decline of chromospheric emission with time. Audard *et al.* (2000) found a scaling between coronal flare rate and underlying stellar X-ray luminosity for a sample of stars including several with ages in this age range. They quantified this as

$$N(> E_c = 10^{32}) = 1.9 \times 10^{-27} L_X^{0.95} \text{ flares per day}, \tag{2.9}$$

where $N(> E_c = 10^{32})$ is the coronal flare rate above a threshold flare energy of 10^{32} erg, and L_X is the star's coronal X-ray luminosity. Ayres *et al.* (1995) and Piters *et al.* (1997) established scalings between coronal emission and different chromospheric emission indicators for cool main-sequence dwarfs, $L_X \propto L_{\text{chrom}}^{y}$, where $y \sim 1.5$ for C IV emission (Ayres *et al.*, 1995), $y \sim 2$ for Ca II HK emission (Piters *et al.*, 1997), and $y \sim 3$ for Mg II h emission (Ayres *et al.*, 1995). Skumanich (1972) showed that chromospheric emission declines roughly with stellar age as $L_{\text{chrom}} \propto t^{-1/2}$. Simplifying these relations to

$$N(> E_c) \propto L_X, \tag{2.10}$$

$$L_X \propto L_{\text{chrom}}^{y}, \tag{2.11}$$

where y takes on different values depending on the chromospheric emission being considered, and

$$L_{\rm chrom} \propto t^{-1/2}, \tag{2.12}$$

suggests that the flare rate may decline with age anywhere from $N(> E_c) \propto t^{-0.75}$ to $N(> E_c) \propto t^{-1.5}$. However, note that Schrijver *et al.* (2012) found that the above scaling between flare rate and coronal luminosity cannot be used to "correct" the flare rate of active stars like those considered in Audard *et al.* (2000) to the solar flare rate via their coronal luminosity. This suggests a breakdown in the validity of a scaling-relation approach.

Single G stars in this age range exhibit flares at least as powerful as the largest solar flares, but occurring several times per day. Audard *et al.* (2000) presented an analysis of EUV flare activity for a sample of late-type stars, including κ Cet, a G5V star with an age of 300–400 Myr (Mamajek and Hillenbrand, 2008). They determine an index to κ Cet's flare frequency distribution, with α greater than 2 (2.2) but with large error bars ($\geq$0.5); using the scaling above between flare rate and X-ray luminosity for κ Cet's X-ray luminosity of 10^{29} erg s^{-1} translates to 6.7 flares per day, above a threshold lower flare energy of 10^{32} erg. κ Cet was also listed as a "superflaring" star in the compilation by Schaefer *et al.* (2000), with an estimated flare energy in the He I D3 line of about 2×10^{34} erg. The dynamic range in the measurements that constitute the flare frequency distribution is not large (only about a factor of 20): some criticisms of the large α index returned by these analyses suggest that other factors (such as a downturn in the intrinsic flare-frequency distribution due to a rollover or cutoff) may be affecting the results.

Solar-neighborhood M dwarfs have historically been the most studied flaring stars: the propensity for dramatic blue–optical flare increases initially brought them to the attention of stellar astronomers but now their flares have been studied across the electromagnetic spectrum. Ages of individual M dwarfs are difficult to ascertain, but most objects are considered to have ages of at least a few hundred Myr to 1 Gyr, so they fall squarely within the age range being considered. There is a range of flare energies observed on dMe (i.e., dwarf M-type stars with emission line features) flare stars: the lowest level detectable X-ray flares from the closest star to the Sun (a flare star – Proxima Centauri), are comparable to M-class solar flares (Güdel *et al.*, 2004; flare energy of $10^{28}-10^{29}$ erg). At the other extreme, the most energetic flares from dMe flare stars are in the $10^{34}-10^{35}$ erg range (Kowalski *et al.*, 2010; Osten *et al.*, 2010). Flares are also very frequent, with flare frequencies of the least energetic flares as often as a few per hour. Figure 2.8 compares the flare frequency distributions for flares of different M spectral type, as well as broken up by activity level (Hilton, 2011). Inactive stars (classed by their low or undetectable quiescent Hα emission levels) have a lower flare rate compared to active stars of

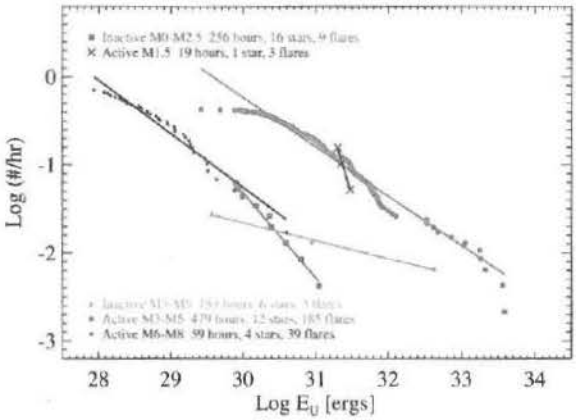

Fig. 2.8 Cumulative flare frequency distributions for different categories of M dwarfs, from the PhD thesis of Eric Hilton. Through long stares at different classes of M dwarfs, the difference in the occurrence rate of flares of different U band energies can be determined.

similar spectral type, with maximum flare energies about an order of magnitude less than those observed on the active M dwarfs.

Flares are even observed to extend into the realm of the ultracool dwarfs: late M dwarfs with photospheric temperatures less than 3000 K (Schmidt *et al.*, 2014). X-ray studies of flares on M dwarfs have considered the flare frequency distribution of individual coronal flares; several studies (Audard *et al.*, 2000; Kashyap *et al.*, 2002) have determined that the shape of the distribution is a power-law with index α greater than 2, which would suggest that flares may be the source of energy required to maintain a corona.

The Hyades cluster is a relatively nearby open cluster of stars with an age of ~800 Myr and has been the subject of multiple flare studies. The flare rate should be lower than for the younger stars considered in the previous section, and the sparseness of flare detections and inability to connect flares in different wavelength regions confounds interpretation. Stelzer *et al.* (2000) studied X-ray flares from a sample of objects in the Hyades as well as nearby stars from younger associations. Figure 2.9 depicts the combined flare rates of objects as a function of age, up to about 1 Gyr, separated by evolutionary status at the youngest ages. The flare rate by 800 Myr is lower than for younger stars. Total integrated energies could not be determined due to the sparse temporal sampling of the data, but the flares represented factors of a few to 20 times increase in the underlying stellar X-ray luminosity. These observations span a range of cool spectral types, and small numbers of detected events prevents exploration of other relevant parts of parameter space like stellar mass and rotation. There is a clear decrease in the flare rate, but whether this is biased by the types of objects detected is not clear. White *et al.*

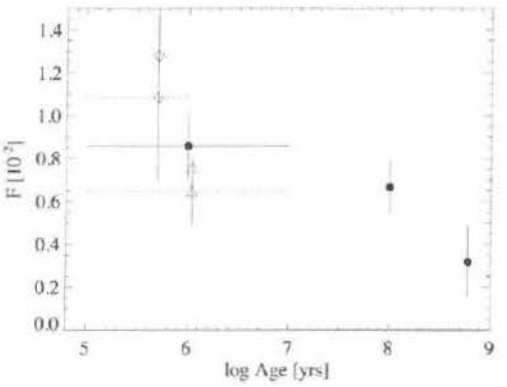

Fig. 2.9 X-ray flare rate expressed as a percent of observing time for stars of different ages, from the study of Stelzer *et al.* (2000). The sensitivity to flares is set to a uniform value to account for the differing distances. Diamonds indicate classical T Tauri stars, triangles indicate weak-lined T Tauri stars. The horizontal line gives the age spread of the young stellar objects. There is a clear drop in flare rate by the age of the Hyades (800 Myr).

(1993) performed a radio study of stars in the Hyades cluster, finding no detections from M dwarfs which have a similar age and rotation rate to the M dwarfs in the solar neighborhood, and with sensitivities sufficient to detect the largest events observed from nearby M dwarfs. They conclude that by the age of the Hyades the activity of most dwarf stars has decreased to a low level where flare rates and energies have fallen below the levels of the nearby population of M dwarf stars. Their results are consistent with expected declines in activity from the age–rotation–activity connection. Browne *et al.* (2009) probed for ultraviolet flares on stars in the Hyades and Pleiades (age ~100 Myr) clusters, using the 1.2° field of view of the GALEX satellite. Most of the variable sources inferred to be flaring are M dwarfs, and only one was a bona fide Hyades cluster member (and an M dwarf). It had a flare with an NUV (1800–2800 Å) energy release of 4.5×10^{29} erg. The event rate is one flare in ≈15 000 s, or a flare duty cycle of 3%, which is clearly elevated compared to the X-ray flare rates in Fig. 2.9. Given the singular nature of the detection it is not possible to extrapolate further on the comparison of X-ray versus ultraviolet flare rates. Concentrated optical observations have returned a range of flare rates for one of the more active Hyades M dwarfs: flare frequencies ranging from 0.09 flares h^{-1} up to 1.25 flares h^{-1} have been measured (Haro and Parsamian, 1969; Rodono, 1974).

2.2.3 Stellar adulthood: 1–5 Gyr

The solar system, and thus the Sun's, age measurement of 4568 Myr (Bouvier and Wadhwa, 2010) fits squarely within the "stellar adulthood" phase of its life.

Detections of flares on stars in this age range are much fewer. The decline of flaring with age is generally assumed to follow the trends of other activity indicators, but whether this is in fact the case is an open question. Evidence that magnetic activity may not decline monotonically at Gyr ages comes from a few sources: Silvestri *et al.* (2005) concluded that chromospheric activity in M dwarfs did not decline in the 1–10 Gyr range as fast as predicted based on extrapolating from objects with ages < 1 Gyr. Studies of chromospheric activity and its dependence on age and rotation led Pace and Pasquini (2004) to conclude that they found no evidence of decay in quiescent chromospheric activity for stars older than a few Gyr; instead, the major decline in activity was in objects at ages of the Hyades and earlier (0.6 Gyr), for clusters of 1.7 Gyr and older (up to 4.5 Gyr) the same activity level was seen. This result was updated by Pace (2013) who found no evidence for a decay of chromospheric activity after about 2 Gyr.

Binarity influences activity and thus flaring rates may remain high for old stars in close binary systems (Rocha-Pinto *et al.*, 2002) which can overestimate the flare rate for stars in this age range, if binarity has not been ruled out. The influence of rotation on activity means that tidally locked binary close systems have significantly enhanced levels of activity. They are frequently observed to undergo enormous outbursts at radio (Mutel *et al.*, 1998) and X-ray wavelengths (Osten *et al.*, 2007), even being picked up by satellites tuned to finding the transient hard X-ray radiation from gamma-ray bursts. The radiated energies approach 10^{38} erg, with flare frequency distributions with a power-law index of near 1.8 (Osten and Brown, 1999). Time scales for these flares can be staggering, often lasting longer than the rotational/orbital period of the system. Owing to their frequent and extreme flares, close binary systems have been popular subjects of study; in contrast with flares on M dwarfs, these flares are most readily studied at radio and X-ray wavelengths due to the small contrast at optical bands. Osten *et al.* (2004) provided a comprehensive discussion of multi-wavelength flare campaigns on one active binary system, HR 1099. Although several trends in these flares suggest an extension of the solar flare analogy, the large difference in observed properties of these flares may give pause to the extent to which the solar/stellar analogy can be stretched (and whether it may break). These stars already produce steady levels of high-energy radiation near the limit of what stars seem capable of maintaining, but flares increase the luminosity above that, often approaching the bolometric luminosity of the system. Correlations between flare frequency and underlying stellar luminosity as found for single active dwarfs in Audard *et al.* (2000) have been found among flares on active binary stars (Osten and Brown, 1999).

Because the flare rate is expected to be low on older stars, a systematic search for flares in an older stellar population needs a large number of stars, and involves

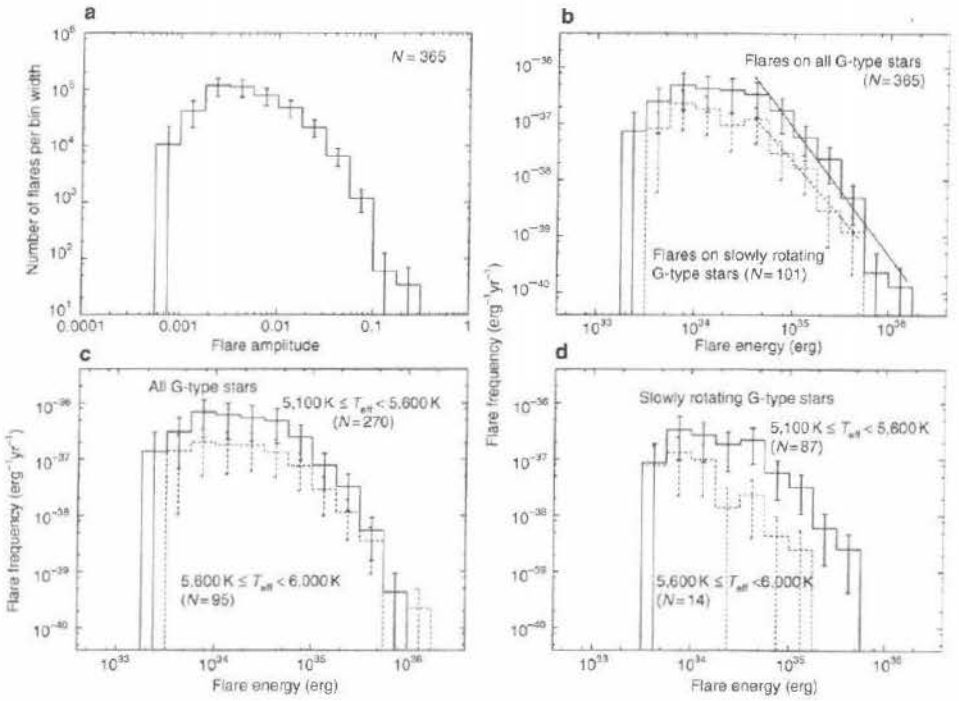

Fig. 2.10 Summary of flare characteristics seen on G-type stars from Maehara *et al.* (2012). (a) The peak flare amplitudes are 10% or less of the star's underlying brightness. (b) The distribution of flares with energy on slowly rotating stars appears similar to that of all G-type stars surveyed. (c) The distribution of flares with energy appears similar when breaking the stars up in hotter vs. cooler stars. (d) The slowly rotating hot stars show a decrease in flare frequency.

a relatively long stare coupled with fast cadence to detect and resolve the flaring emission from any other variability. The Kepler spacecraft's exquisite photometry can be re-purposed from finding evidence of transiting extrasolar planets around stars to looking for rare short-time-scale flaring events on the stars themselves. Maehara *et al.* (2012) reported on energetic flares found from a sample of G-type stars in the Kepler field of view (see Fig. 2.10). While the ages of the individual stars are not known, the spread of rotation periods, particularly the continuing trend of flares on stars with rotation periods longer than 10 days, suggests an intermediate to old age. Further follow-up by Nogami *et al.* (2014) finds flares on two G-type stars with rotation periods of 21.8 and 25.3 days, near the solar value, and thus approximately solar age. The energetics of these flares is large, with minimum flare energies in the range 10^{33} erg, and extending up to 10^{36} erg. The distribution has a power-law index of -2.3 ± 0.3 for superflares found on all G stars, and -2.0 ± 0.2 for slowly rotating G stars, above 4×10^{34} erg.

2.2.4 Stellar old age: beyond 4.5 Gyr

The age of the Sun is pegged to the age of the solar system, and so consideration of stars older than the Sun technically is beyond the scope of this chapter if we look at the history of the Sun. For completeness we include these old stellar ages because there are observations demonstrating the continuation of flaring activity into this regime, and it is of interest to know what the Sun may have in store for the solar system over the coming billions of years.

That magnetic activity can survive to such old ages is evidenced by the flare observed serendipitously on the old solar neighborhood M dwarf Barnard's star, at an estimated age of 11–12 Gyr (Paulson *et al.*, 2006). Because M dwarfs are presumed to carry magnetic activity for longer time scales this is perhaps not surprising. The event had incomplete coverage due to its serendipity, and the flare was identified through the increase in Balmer lines and continuum enhancements. Although noting that such events are likely rare in such old stars, Paulson *et al.* (2006) point out two other references in which observations of flares on Barnard's star are noted, so they may not actually be that uncommon.

Osten *et al.* (2012) re-purposed an observation designed to find eclipsing extrasolar planets in a 10-Gyr stellar population in the Galactic bulge, and used it to study the incidence of optical flares in an old stellar population (see Fig. 2.11). The majority of the flaring stars could be associated with stars at the distance and age of the Galactic bulge, indicating that flaring variability can be maintained. A large fraction of the stars exhibited large-scale photometric modulations (in addition to

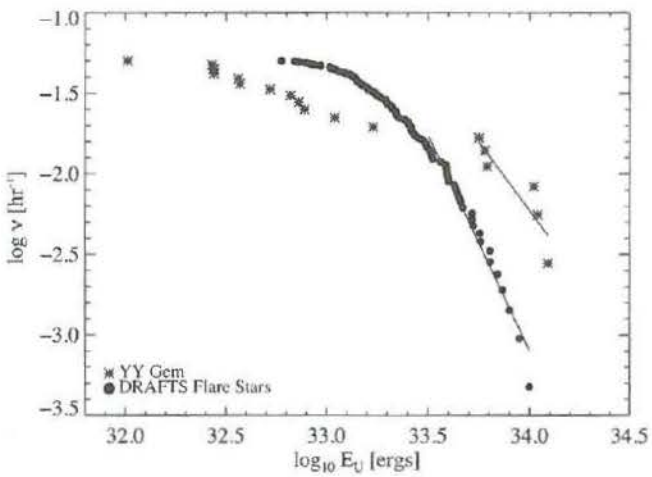

Fig. 2.11 Flare frequency distribution of flares observed on 10-Gyr stars in the Galactic bulge. (From Osten *et al.*, 2012.)

the flaring variations), which indicate rotation periods of a few days. The supposition is that both types of stellar variability can be explained due to the survival of magnetic activity on stars found in tidally locked binary systems, in which the space motions or kinematics indicate an old age but the activity indicators suggest youth.

2.3 Take-away points

The central thesis of this chapter is that studies of flares on stars other than the Sun can be used to give insight into flares on the Sun, and thus extend the time baseline for examining the influence of the Sun on its environs, as well as studying the influence that other host stars may have on their planets as a function of evolutionary time. This approach suffers from some biases in the observations of stars: the types of stars which are the best studied for their flares tend not to be exact replicas of the Sun. M dwarfs, tidally locked active binaries, or young stars with disks have the best characterization of their flares. The wavelength ranges used for studies of stellar flares are often not the same as those used for solar-flare studies, and so an intercomparison requires a conversion to the same wavelength range, after accounting for energy partition. Because of the astronomical difference between our closest star, the Sun, and the distances of even the most nearby stars, there will always be sensitivity differences between solar- and stellar-flare studies; at best, stellar-flare studies can hope to probe the region of the largest solar-flare events.

Nevertheless, despite the possible pitfalls in such an approach, detailed studies of the flares on these stars show agreement with solar flares, indicating that the same physical processes are occurring during solar and stellar flares. Flares are tracers of time-dependent magnetic activity, and exhibit trends with some diagnostics of steady-state magnetic activity, such as the correlation between coronal flaring and underlying coronal emission noted earlier. Assuming that such scaling laws are valid enables an opening of the parameter space. Observations of ensembles of stars can gain insight into the gross flaring properties of these stars, where such conclusions may not be evident from observations of a single star due to the low flaring rate per star.

While we still do not have detailed characteristics (including all relevant flare processes) of a true solar analog at various stages in stellar evolution, the vast astronomical discovery space does enable a reasonable picture to be painted of how the Sun's flaring activity changed over the course of its time, and even predicts what lies in its future. Outstanding issues include incomplete sampling of flares in both wavelength space, and as a function of stellar type, for stars of different ages and rotation rates.